Journal of The Electrochemical Society, **147** (12) 4432-4439 (2000)
S0013-4651(99)11-004-8 CCC: $7.00

Characterization of Metal Hydride Electrodes via Microperturbation and *In Situ* Intrinsic Resistance Measurement

Chunsheng Wang,[a,*,z] Andre Rakotondrainibe,[a,*] A. John Appleby,[a,*] and Frank E. Little[b]

[a]*Center for Electrochemical Systems and Hydrogen Research, and* [b]*Center for Space Power, Texas Engineering Experiment Station, Texas A&M University, College Station, Texas 77843-3402, USA*

Microperturbation methods, including galvanostatic intermittent titration using applied microcurrent pulses (GIT), small amplitude cyclic voltammetry, and electrochemical impedance spectroscopy (EIS), together with *in situ* intrinsic (*i.e.*, physical) resistance measurements, have been applied to investigate charge/discharge kinetics of a $LaNi_{4.4}Sn_{0.25}$ metal hydride (MH) electrode as a function of cycling. The results show that electrode capacity loss was caused by reduced ability to absorb hydrogen. High frequency semicircles in the Nyquist plots may be attributed to hydrogen transition between the adsorbed and the absorbed states, and are unrelated to contact resistance between the current collector and the hydride particles, although this showed contact resistance between alloy particles and current collector. This contradicts a generally accepted interpretation of EIS data. It was difficult to obtain hydrogen diffusion resistance from EIS results when the potential change in the electrode charge-discharge plateau is smaller than the EIS voltage perturbation, because long charge/discharge times in the low frequency range change the state of discharge. Alternating current EIS is more suitable than alternating voltage studies to investigate hydrogen diffusion kinetics in MH alloys with a flat potential plateau. Similarly, it is also difficult to obtain hydrogen diffusion resistance from small amplitude cyclic voltammetry because of the size of the charge/discharge capacitance. However, the total reaction resistance may be obtained from GIT.

Manuscript submitted November 1, 1999; revised manuscript received July 20, 2000.

Sealed nickel metal hydride (NiMH) secondary batteries have been developed and commercialized in recent years to replace nickel-cadmium (NiCd) batteries for many applications because of their high energy density, high rate capability, tolerance to overcharge, deep discharge capability, and lack of toxic heavy metals.[1]

Extensive work has been performed on MH electrode kinetics,[2-13] but there is disagreement on the interpretation of results. It is generally believed that when a small anodic perturbation is applied to the hydride electrode, a charge-transfer step occurs which involves transition of hydrogen between an absorption site near the surface to an adsorbed site at the surface, followed by diffusion of absorbed hydrogen from the bulk to the first site. The exchange current for the charge-transfer step can be calculated from small amplitude cyclic voltammetry (SACV) [or linear micropolarization resistance ($\eta <$ 10 mV)][3-9] and from electrode impedance spectra (EIS).[7-13] However, the exchange currents obtained from the two methods differ,[4] although they should be the same according to the established theoretical relationship of SACV to EIS.[14] Experimental data[7] and a theoretical analysis[9] show that linear micropolarization gives the total resistance of the hydriding-dehydriding reactions, and it reduces to the exchange current only when the electrochemical reaction is rate-determining.[9] EIS is an effective technique for kinetic analysis because it can give the individual resistances for each hydride electrode step if these have different time constants.[7-12] However, different interpretations of Nyquist data have been given, *e.g.*, Kuriyama *et al.*[12,13] and Zheng *et al.*[8] attribute the high frequency semicircle to the resistance and capacitance of the current collector-alloy powder pellet contact. The midfrequency semicircle was attributed to the impedance between electrode particles, the low frequency arc to interfacial charge transfer, and that of the low frequency slope to a Warburg diffusion impedance. However, theoretical analysis[10] and simulations[11] suggest that the semicircle in the high frequency range is due to hydrogen transition between absorption and adsorption.

Measurement of contact resistance between the current collector and active alloy particles was therefore required to investigate its effect on EIS results. An *in situ* resistance measurement method was used to investigate kinetics of metal hydride electrodes as a function of time in this work. The reaction resistance of $LaNi_{4.4}Sn_{0.25}$ electrodes measured using EIS, SACV, and galvanostatic intermittent titration (GIT) using applied microcurrent pulses (*i.e.*, galvanostatic microdischarge as a function of state-of-charge, SOC) are compared.

Experimental

Preparation of alloy powder and electrodes.—Alloy ingots of composition $LaNi_{4.4}Sn_{0.25}$ were prepared by arc melting the components and annealing for 72 h, both under helium atmosphere, and mechanical pulverizing to *ca.* 40 μm particle diam. Hydride electrodes were prepared from a 50-33-17 wt % mixture of alloy powder, Vulcan-XC-72 conducting furnace black (Cabot Corporation), and polytetrafluoroethylene (PTFE). Nickel mesh current collectors were pressed into each side of an alloy pellet of 2 cm^2 geometric area with a thickness of 1.35 mm (about 20.25 mAh total capacity, 75 mg alloy weight). The hydride anode was placed in the center of a four-compartment glass cell, which had two large area $Ni(OH)_2$/NiOOH electrodes (Hughes Aircraft Company) on either side, and an Hg/HgO reference electrode in the fourth compartment. The 31 wt % KOH electrolyte was prepared from reagent grade material and deionized water. Before experiments, electrodes were immersed in the electrolyte for at least 4 h for impregnation.

To avoid confusion over the various electrode resistances discussed here, the expression intrinsic resistance is used below to refer to those physical elements of resistance which are present within the thickness of the electrode, excluding any electrochemical (faradaic) elements. These include the electronic resistance of the series parallel array of hydride particles themselves, the transmission line of various contact resistances between the particles, including electronic contacts with and within the binder and ionic (electrolytic) contacts, and the electronic resistances of the current collectors and the contact resistances between them and the neighboring hydride particles. This intrinsic resistance may be evaluated by an *in situ* direct current method.

Electrochemical charge/discharge cycling.—Electrodes were charged at 100 mA/g for 3.5 h and discharged at 50 mA/g to an end-of-discharge potential of −0.6 V *vs.* Hg/HgO at room temperature using an Arbin Corporation (College Station, TX) automatic battery cycler. Between charge and discharge, the electrodes were left at open circuit for 20 min (to allow the potential to reach a stable value) to monitor the stable potential at full charge and complete discharge, and to measure the resistance of the hydride electrode without interrupting the charge-discharge current. Two identical electrodes were chosen for electrochemical measurement. The first was cycled 35

* Electrochemical Society Active Member.
z E-mail: cswang@pop.tamu.edu

S0013-4651(99)11-004-8 CCC: $7.00

times without interruption, whereas the second was cycled five times, then disconnected and compressed between two PTFE holders containing small holes to allow entry of electrolyte. EIS, GIT, SACV, and *in situ* intrinsic resistance measurements were performed on this electrode before and after compression. Following this, cycling was continued on the compressed electrode.

In situ intrinsic resistance of hydride electrode.—In situ intrinsic resistance measurements used the arrangement in Fig. 1. One potentiostat was used for charge-discharge of the electrode, and another measured intrinsic resistance. For this, a constant current of 10 mA was passed through the hydride electrode, and the intrinsic resistance was determined from the voltage difference across it.

EIS measurement.—Electrochemical impedances were measured from 65 kHz to 1 mHz at 5 mV potentiostatic signal amplitude or 0.5 mA galvanostatic amplitude, using a Solartron FRA 1250 frequency response analyzer and a Solartron model 1286 electrochemical interface. Before EIS measurements, the electrodes were left at open circuit for 20 min to allow the electrode potential to stabilize.

SACV.—SACV measurements used electrode potential scanning at 1 mV/s at overpotentials less than 10 mV. The polarization resistance can be generally calculated from the current-potential (I-E) slope. Because of the long relaxation time at high states-of-discharge (SODs), the polarization resistance was determined from this slope at an overpotential of approximately 9 mV. Scan rates of 0.5, 0.1, 0.05, and 0.01 mV/s were used to investigate the influence of this parameter on measured resistance.

GIT.—GIT using applied microcurrent pulses (galvanic microdischarge as a function of SOC) was carried out on initially fully charged electrodes by alternating a pulse discharge at 25 mA/g for 20 min, then leaving the electrode at its (constant) rest potential for the same time. The rest time between successive dehydriding steps was determined to be rather critical, since it must be sufficiently long to establish (pseudo)equilibrium, but short enough so hydrogen self-discharge was not significant. The total measurement time for the $LaNi_{4.4}Sn_{0.25}$ electrodes examined was 22 h, and self-discharge measurements showed that only 3.5% of total hydrogen was lost during this time. The hydrogen desorbed in each pulse was 8.33 mAh/g, so the equilibrium potential and the *in situ* intrinsic resistance (defined above) as a function of hydrogen content could be readily obtained. These measurements may be used to construct equilibrium potential-composition-temperature (PCT) isotherms of hydride electrodes (PCT diagrams), which are thermodynamically related to the equilibrium hydrogen pressure by the Nernst equation[4,15-17]

$$E_o\ (vs.\ \mathrm{HgO/Hg}) = -0.9324 - 0.0291 \log(p_{H_2}) \qquad [1]$$

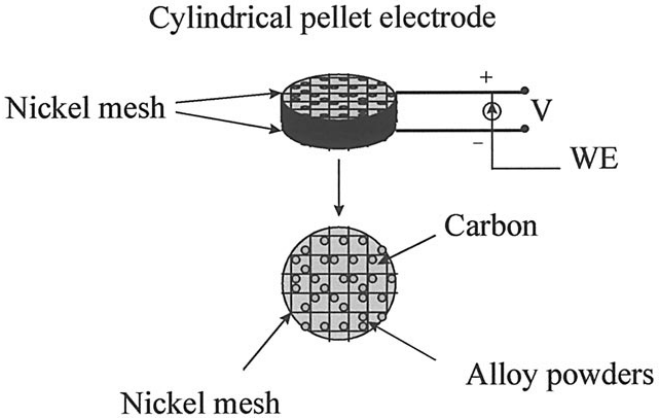

Figure 1. Schematic of *in situ* intrinsic resistance measurement of metal hydride electrode. In some cases, the electrode was compressed on each side by two PTFE holders containing small holes to allow penetration of electrolyte.

Using the GIT technique and Eq. 1, Ratnakumar *et al.*[4] and Iwakura *et al.*[17] have successfully measured the equilibrium PCT isotherms of $LaNi_{5-x}Sn_x$ alloy ($0.1 < x < 0.3$) 4, $LaNi_{5-x}M_x$ (M = Ni, Cu, Cr, Mn, and Al) [17] and compared them to gas phase isotherms of the same alloy. They found that the discharge equilibrium PCT isotherms show a resemblance to the gas-phase isotherms.[4,17] Therefore, the PCT isotherms for $LaNi_{4.4}Sn_{0.25}$ given here, as measured by GIT during the discharge process represent equilibrium potentials. Moreover, the reaction resistance of the dehydriding reaction as a function of hydrogen content can be directly calculated from the overpotential-discharge current (1.88 mA) slope at the small total overpotential used (<10 mV).[18] As measured, this resistance included part of the electrolytic solution resistance, charge transfer resistance, and hydrogen diffusion resistance.

Results and Discussion

Charge/discharge stability of the $LaNi_{4.4}Sn_{0.25}$ electrode.—The change in electrode potential during a charge-discharge cycle is shown in Fig. 2. In it, E_1 is the potential at the end of charge. E_2 is the open-circuit potential of the fully charged electrode after 20 min at open circuit, and E_3 is corresponding potential for the fully discharged electrode. Since E_2 is stable under the above conditions (*i.e.*, it may be regarded as an equilibrium potential, E_{eq}), the difference between E_1 and E_2 is the hydrogen evolution overpotential at a charge current density of 100 mA/g. The *in situ* intrinsic resistances of the electrode in the fully charged and fully discharged states (R_1 and R_2) were measured at E_2 and E_3 during the 20 min relaxation periods. Figure 2 shows that the i*n situ* intrinsic resistance initially increases somewhat, and then decreases with increase in alloy hydrogen content, finally stabilizing on full charge. The small initial increase may be the difference between the electronic resistance of the alloy and alloy hydride phases, while the subsequent decrease may be the result of volume expansion and improved contact on hydriding. The corresponding gradual increase, then decrease, in *in situ* intrinsic resistance during discharge is due to volume shrinkage and phase transformation. Figure 3 shows the discharge capacity, *in situ*

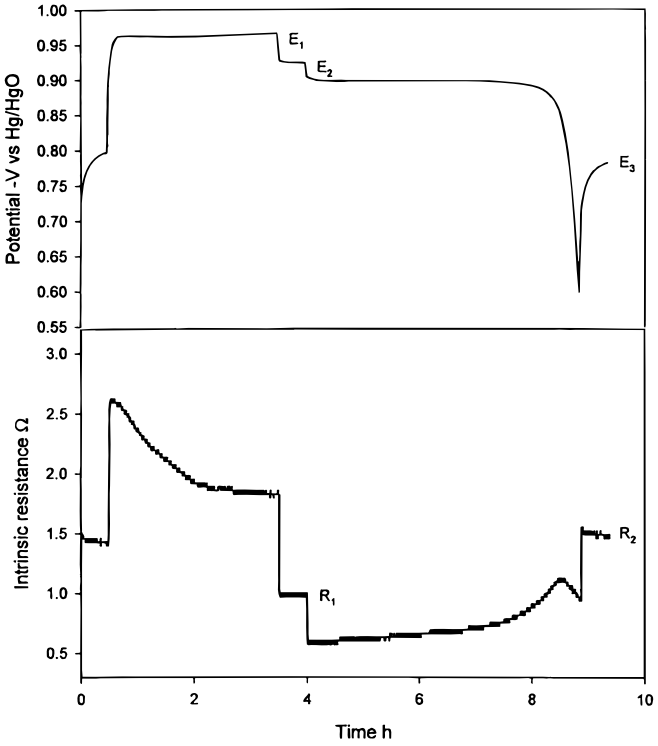

Figure 2. Typical potential and contact resistance profile for a $LaNi_{4.4}Sn_{0.25}$ electrode during a charge-discharge cycle. Charge current: 100 mA/g, discharge current: 50 mA/g.

S0013-4651(99)11-004-8 CCC: $7.00

intrinsic resistance, and potential of the electrode as a function of charge/discharge cycle number. The discharge capacity reaches 252 mAh/g due to alloy activation (pulverization) during the first six cycles, and then it decreases almost linearly to about 140 mAh/g after 35 cycles. $LaNi_{4.4}Sn_{0.25}$ particles may carry an oxide film formed during exposure to air after preparation. The oxide film, and the large particle size of the alloy as prepared, both reduce hydrogen absorption and result in a high hydrogen evolution overpotential. The increase in surface area during the first six cycles is shown by the decrease in both E_1 (the hydrogen evolution potential) and in E_3 (the equilibrium potential of a nominally fully discharged electrode), as Fig. 3 shows. After activation, E_1 becomes rather stable, showing only a slight increase on further cycling.

Figure 4 shows the equilibrium potential after activation *vs.* hydrogen content of the $LaNi_{4.4}Sn_{0.25}$ alloy, which has a flat potential plateau. The figure indicates that the alloy shows a rapid fall in equilibrium potential at hydrogen contents below 50 mAh/g. Hence, the experimental value of E_3 (the equilibrium potential of a nominally fully discharged electrode) indicates the amount of hydrogen remaining in the electrode after "full discharge." The high E_3 potential during initial cycling (Fig. 3) indicates that the oxide film on the initially large alloy particles inhibits hydrogen desorption as well as adsorption. The rapid decrease in E_3 by activation during the first six cycles shows that hydrogen desorption occurs more readily due to more rapid kinetics after pulverization. E_3 begins to increase after six cycles, and then slowly decreases after 15 cycles. It is possible that disintegration of the alloy is responsible for the provisional increase in E_3, because R_1 (*i.e.*, the intrinsic electrode resistance of the fully charged electrode) also increases rapidly during the same period (Fig. 3).

Pulverization of the alloy during activation decreases its ability to absorb hydrogen from the thermodynamic viewpoint and its kinetic polarization, but increases its *in situ* resistance. The effects of pulverization on the charge-discharge characteristics of this hydride alloy are enhancement of both hydrogen electrocatalytic activity and hydrogen diffusion due to decreasing alloy particle size, with a corresponding increase in corrosion rate with increasing surface area. However, alloy corrosion has little influence on surface electrode kinetics (hydrogen electrocatalysis) because E_1 is almost stable during this period. Further, the small decrease in E_3 after 15 cycles implies that discharge kinetics of the alloy increase on further cycling. Similar results have been reported by Zhang *et al.*[19] In Fig. 3 the very small increase in E_2 (*i.e.*, the equilibrium potential of the fully charged electrode) may result from the presence of a newly formed oxide film on the electrode. Pulverization of the alloy can be more easily inferred from the *in situ* resistance measurements, as Fig. 3 shows. Volume expansion during charge following shrinkage during discharge is the most logical explanation for the lower and higher respective *in situ* intrinsic resistances. Pulverization during activation increases the *in situ* resistance change between the fully charged and fully discharged states due to the resulting increase in charge-discharge capacity, and to increasing separation of the alloy particles, so the difference between R_1 and R_2 increases during activation. After the discharge capacity reaches its maximum value, any further pulverization will increase the *in situ* resistance R_2. After 10 cycles, both R_1 and R_2 increase at almost the same rate.

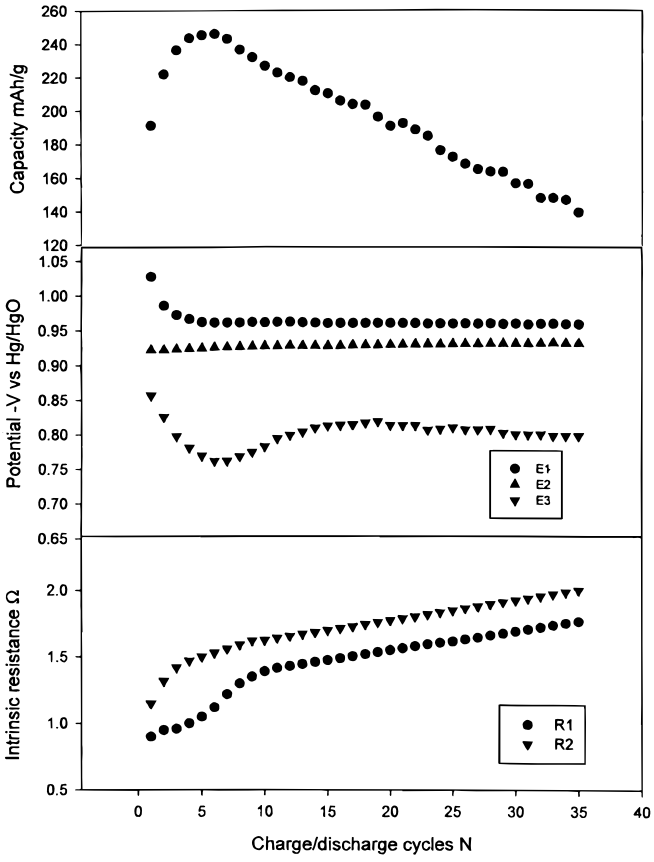

Figure 3. The dependence of discharge capacity, potential, and intrinsic resistance on charge-discharge cycling.

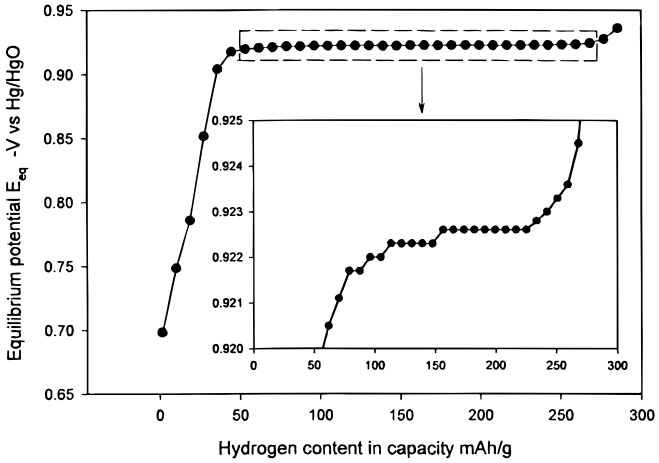

Figure 4. Equilibrium potential (E_{eq}) *vs.* hydrogen content of $LaNi_{4.4}Sn_{0.25}$ electrode after activation. The curve was measured during the discharge process. The inset is an expended part of potential plateau region.

Figure 5 shows the influence of pulverization of $LaNi_{4.4}Sn_{0.25}$ on the electrode cycle life. As already stated, the electrode was first cycled without compression until it reached its maximum capacity, after which the electrode was compressed on each side using two PTFE holders containing small holes to allow entry of electrolyte. It was then cycled a further 45 times. A comparison of Fig. 3 and 5 shows that compression of the MH electrode had the following effects: (*i*) A slight increase in the cycle life; and (*ii*) an increase in hydrogen evolution overpotential, together with a decrease in E_3 with the elimination of the increase in E_3 after activation. E_3 decreases on charge-discharge cycling for both uncompressed and compressed electrodes, which reflects the capacity decline resulting mainly from the decrease in hydrogen absorption capability, but not in decreased hydrogen desorption kinetics. To confirm these results, EIS and GIT with applied microcurrent measurements were conducted on the compressed electrode at 6 and 45 cycles to investigate the absorption capability and kinetics of the electrode.

Figure 6 shows Nyquist plots of the electrode in the 50% discharged state at 6 and 45 cycles, and Fig. 7 shows equilibrium potential *vs.* hydrogen content at 6 and 45 cycles. The equilibrium potential *vs.* hydrogen content of $LaNi_{4.4}Sn_{0.25}$ at 6 cycles in Fig. 7 is close to that of $LaNi_{4.7}Sn_{0.3}$, as reported by Ratnakumar *et al.*[4] The potential of $LaNi_{4.4}Sn_{0.25}$ in the fully charged state is around

S0013-4651(99)11-004-8 CCC: $7.00

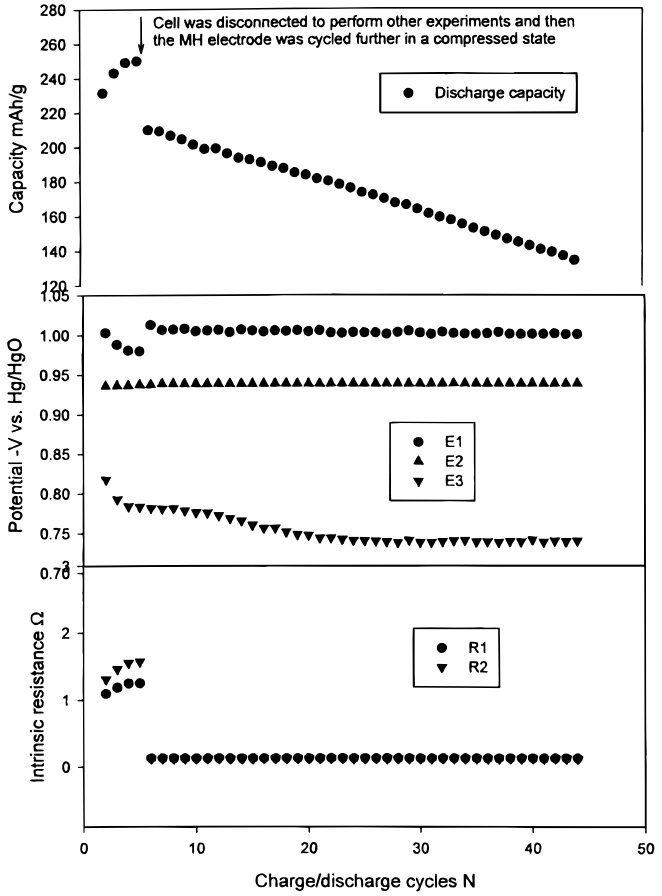

Figure 5. The dependence of electrode discharge capacity, potential and intrinsic resistance on charge-discharge cycle number. The electrode was compressed on each side by two PTFE holders (see Fig. 1) after five cycles.

−0.938 V, which is near the equilibrium potential of a generic hydride electrode in the fully charged state (−0.9324 V *vs.* Hg/HgO from Eq. 1). A slightly more negative potential than the equilibrium value may be related to oxide film formation on the $LaNi_{4.7}Sn_{0.3}$ electrode surface, which may inhibit gaseous hydrogen evolution. As is expected, the hydrogen absorption capability decreases substantially from 288 mAh/g at 6 cycles to 148 mAh/g at 45 cycles. However, the total reaction resistance of the two semicircles in Fig. 6 only decreased from 5.7 to 5.4 Ω. The thermodynamic equilibrium PCT isotherm (Fig. 7) and EIS (Fig. 6) results at different cycle times reconfirmed that the charge/discharge cycle stability is controlled by the decline in hydrogen absorption capability.

EIS characterization.—Previous research in this Center has shown that the metal hydride electrodes are stable and linear systems, which show little change during the periods required for EIS studies.[8] This has been confirmed by Kramers-Kronig transforms.[8] Impedance spectra of a $LaNi_{4.4}Sn_{0.25}$ electrode measured at 50% charge state using descending and ascending frequencies (between 65 kHz and 0.001 Hz) are nearly identical (Fig. 8), which further confirmed that the $LaNi_{4.4}Sn_{0.25}$ electrode has satisfied the stability constraint for EIS measurement. Similarly, EIS data measured under these conditions using different excitation voltages (3 to 10 mV) confirm that the EIS response of $LaNi_{4.4}Sn_{0.25}$ is also linear. Figure 9 shows Nyquist plots for charge-discharge of the same $LaNi_{4.4}Sn_{0.25}$ electrode as in Fig. 5, at six cycles but before compression. Each plot consists of two depressed semicircles, and a Warburg slope *W*. The

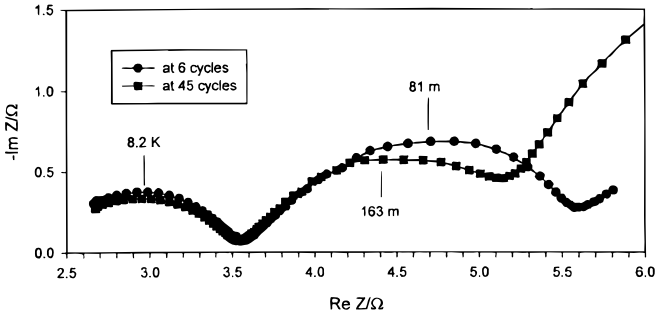

Figure 6. Nyquist plots for $LaNi_{4.4}Sn_{0.25}$ electrode at 6 and 45 cycles. The electrode was cycled in the compressed state.

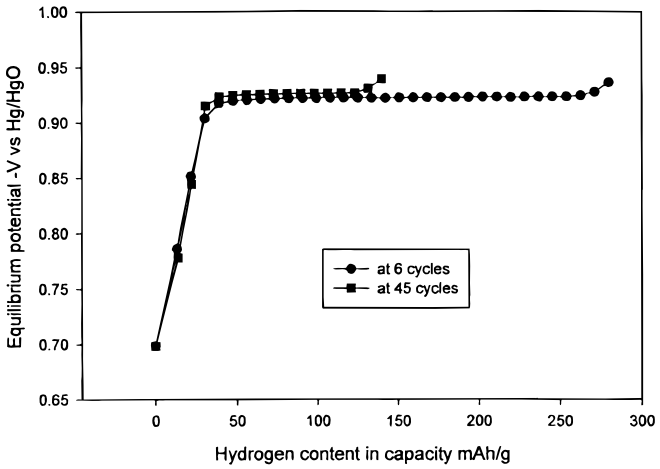

Figure 7. Equilibrium potential *vs.* hydrogen content for $LaNi_{4.4}Sn_{0.25}$ electrode at 6 and 45 cycles. The electrode was cycled in the compressed state.

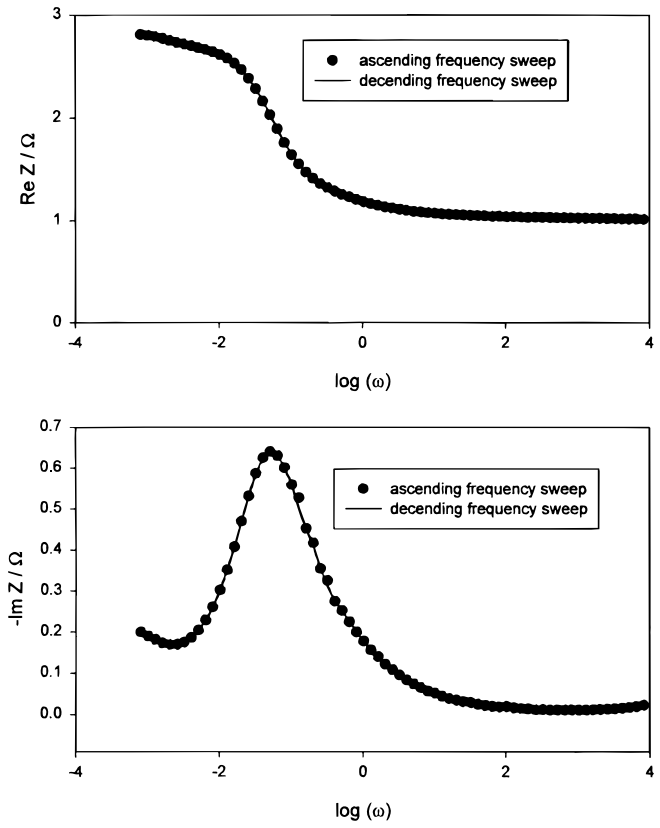

Figure 8. Bode plot of $LaNi_{4.4}Sn_{0.25}$ electrode impedance spectra using ascending and descending frequency sweep at 50% discharge.

S0013-4651(99)11-004-8 CCC: $7.00

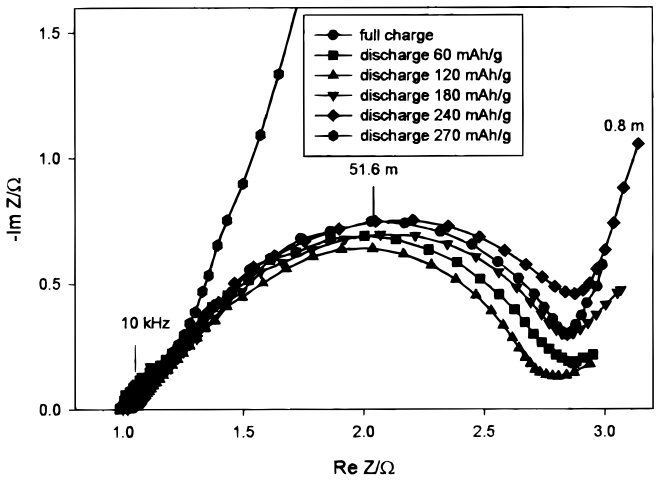

Figure 9. Nyquist plots showing reaction impedance of $LaNi_{4.4}Sn_{0.25}$ electrode in different discharge states. Before EIS measurements, the electrode was fully activated. The numbers in the plots indicate frequency.

semicircle in the low frequency range is SOD dependent, *i.e.,* the size of semicircle decreases with discharge capacity until about 120 mAh/g is reached, then it begins to increase with further discharge. It is generally believed[4,5,7-8] that the semicircle in the high frequency region results from the *in situ* resistance and capacitance between the current collector and the alloy powder pellet. The semicircle in the low frequency region is attributed to the charge transfer resistance and double layer capacitance, whereas the sloping line is the Warburg diffusional impedance. However, other reports[9-11] relate the high frequency semicircle in the high to the hydrogen absorption and desorption reaction.

To investigate the *in situ* intrinsic resistance of the electrode, EIS was performed on two sides of the electrode in the same state of charge. Figure 10 shows Nyquist plots of the intrinsic impedance of $LaNi_{4.4}Sn_{0.25}$ electrode. This shows two resistance-capacitance semicircles in series with an inductive reactance. The semicircle in the high frequency range is independent of SOD, but the low frequency semicircle is sensitive to SOD. These may be compared with an EIS of the electrode obtained after immersion in 6 M KOH for 4 h, but before charge-discharge cycling (Fig. 11). No semicircles are seen under these conditions, and the resistance (determined from the intersection of the high frequency line with the real axis in the complex impedance plot) is almost the same as that in Fig. 10. This resistance may be attributed to the electronic resistance of the MH electrode. Since volume expansion and shrinkage during charge-discharge cycling increased the intrinsic resistance (Fig. 3), it is reasonable to interpret the two semicircles as resulting from contact be-

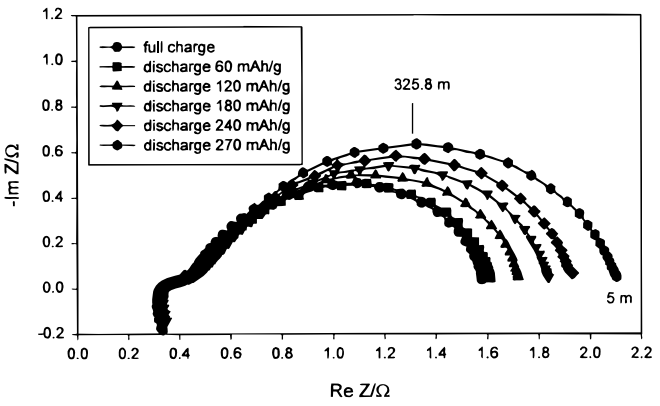

Figure 10. Nyquist plots showing contact impedance of $LaNi_{4.4}Sn_{0.25}$ electrode in different discharge states. Before EIS measurements, the electrode was fully activated. The numbers in the plots indicate frequency.

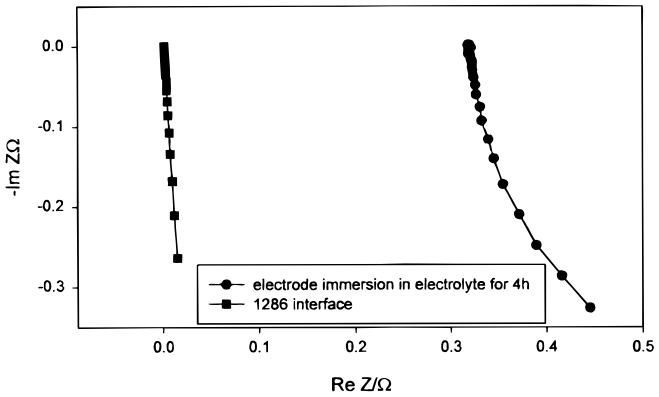

Figure 11. Nyquist plots showing contact impedance of $LaNi_{4.4}Sn_{0.25}$ electrode after immersion in the electrolyte for 4 h. Nyquist plots of connected CE/RE_1 and WE/RE_2 outlets in the Solatron electrochemical interface model 1286 are also shown for comparison after the two groups of terminals were connected together (instrumental artifact).

tween the current collector to the alloy powder, and to particle to particle resistance of the alloy powder, respectively. The inductive reactance in the high frequency range is not associated with the MH electrode, but is an artifact resulting from the Solartron equipment used (it appears if CE is connected to RE_1, *WE* to RE_2, and then they are all connected together, as Fig. 11 shows).

Figure 12 shows Nyquist plots for the reaction impedance of the $LaNi_{4.4}Sn_{0.25}$ electrode after compression by two PTFE holders, as indicated earlier. On comparing the EIS results for the electrode before and after compression (Fig. 9 and 12), the following difference may be observed: (*i*) the diameter of high-frequency semicircle increases after compression, and (*ii*) a small increase in solution resistance occurs after compression due to the slight increase in the distance between the hydride and reference electrodes after compression. Although contact resistances exist between the current collector and the MH powder, it is difficult to attribute the high frequency semicircle (Fig. 9) to a contact resistance for the four following reasons: (*i*) the total contact resistance in Fig. 10 is much higher than the resistance shown in the high frequency range in Fig. 9; (*ii*) the characteristic frequency (325.8 mHz) in Fig. 10 is much smaller than that (10 kHz) in high frequency range in Fig. 9, (*iii*) compressing the electrode reduced the intrinsic electrode resistance (comparison of Fig. 10 and 13) but increased the resistance in the high frequency range (comparison of Fig. 9 and 12), and (*iv*)

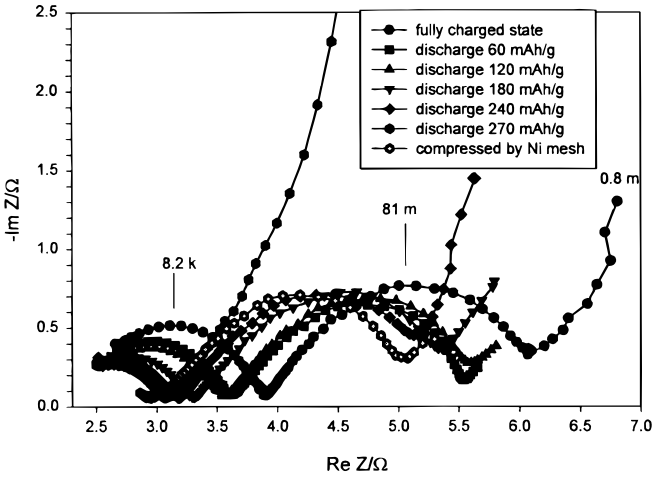

Figure 12. Nyquist plots showing reaction impedance of $LaNi_{4.4}Sn_{0.25}$ electrode at different discharge states. The electrode was compressed on each side by two PTFE holders (Fig. 1). The numbers in the plots indicate frequency.

S0013-4651(99)11-004-8 CCC: $7.00

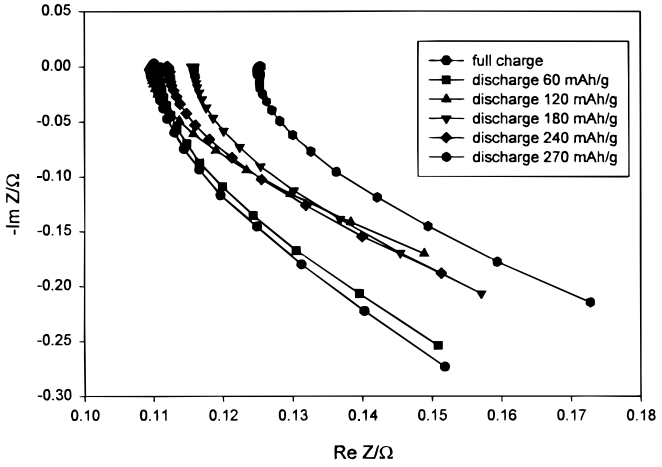

Figure 13. Nyquist plots showing contact impedance of $LaNi_{4.4}Sn_{0.25}$ electrode at different discharge states. The electrode was compressed on each side by two PTFE holders (as Fig. 12).

after compression, the resistance in the high frequency range of Fig. 12 decreased with SOD, but the intrinsic electrode resistance (including contact resistance) in Fig. 13 increased with SOD. Figure 12 also shows that the diameters of the high frequency semicircles were very small if the electrode was compressed by nickel mesh instead of PTFE. This shows that this semicircle is related to the hydrogen absorption process, and can be attributed to hydrogen transitions between the absorbed and adsorbed states.

The impedance for finite spherical diffusion of hydrogen into a metal hydride electrode with a flat potential plateau should be a Warburg impedance in series with a capacitance in the high frequency range, with a resistance in parallel with a series resistance-capacitance.[10] However, the impedance for hydrogen diffusion shows only a Warburg slope because the frequency is not sufficiently low to correspond to the characteristic frequency for hydrogen diffusion in the alloy particles (Fig. 9). When the frequency was further decreased to 0.4 mHz, a noise line appeared (Fig. 12 and 14) because the signal amplitude (5 mV) was larger than the potential change in the potential plateau region (see Fig. 4), *i.e.*, the signal can completely charge and discharge the hydride electrode over a complete 41 min cycle at 0.4 mHz. Hence, no usable data can be obtained under these conditions. This problem may be solved by using an alternating current (ac) signal instead of alternating voltage (av) for EIS determination. Figure 14 shows a comparison of EIS using av and ac signals. As expected, the av impedance shows noise at low frequency, but a semicircle appears in ac impedance spectroscopy. The present work thus validates the theoretical EIS model of the hydride electrode given previously,[10] *i.e.*, the two high frequency semicircles may be attributed to hydrogen transition between absorbed and desorbed states, and to the charge transfer reaction, respectively, the relative frequencies depending on the reaction rate constants in the usual way. A sloping line followed by a low frequency semicircle corresponds to hydrogen diffusion. A simple equivalent circuit of the hydride electrode[10] is shown in Fig. 15, where R_s, R_{ct}, and R_{ht} are the solution-, charge-transfer-, and hydrogen-transfer resistances, respectively; and C_{dl} and C_{ht} are the double layer and absorption capacitances, respectively. A diffusional resistance (R_d) is in parallel with a series resistance-capacitance (R) and (C_d), and corresponds to the impedance of the hydrogen diffusion at low frequency. The circuit differs from that of Kuriyama *et al.*,[12] but has many of the same physical attributes, such as two high frequency semicircles and a hydrogen diffusion impedance. The only difference is in the properties of the semicircles in the high frequency region. The difference should not be perceived too critically, since all equivalent circuits in complex systems involving transmission line phenomena are necessary approximations. Similarly, the intrinsic impedance of the hydride electrode can be simply considered as two *R-C* elements in series. Although the *R-C* equivalent circuit of metal-hydride electrode has been established from a small amplitude sine wave perturbation as a function of frequency, it is also suitable to interpret other time dependent microperturbation techniques, such as pulsed microcurrent and SACV.

Intrinsic and reaction resistance during discharge via GIT.—This was carried out using repeated 1.88 mA anodic current pulses, each lasting 20 min. The current and time were chosen to provide a measurable perturbation with minimum self-discharge during measurement. Microcurrent pulse measurement is a useful technique because both the electrochemical reaction resistance and the intrinsic resistance can be obtained simultaneously. The constant current of 10 mA applied between both sides of the electrode to measure the intrinsic resistance has no influence on hydrogen content, and the resulting small voltage across the two sides of the electrode has little influence on the measurement of reaction resistance because the latter depends only on the overpotential resulting from applying the current pulse. In fact, the resistances measured with and without a 10 mA dc current passing through the electrode were almost identical. This method also allows measurement of the intrinsic resistance across the electrode when it is nominally at open circuit.

Figure 16 shows the typical decay of potential and resistance as successive current pulses are applied. By analyzing the equilibrium potential and overpotential at different hydrogen contents it is possible to obtain both the equilibrium potential *vs.* hydrogen content curves (PCT curves) and the reaction resistance *vs.* hydrogen content curves at a given temperature. The reaction resistance, obtained from the overall overpotential divided by the discharge current, is the total of part of the electrolyte solution resistance, the charge transfer resistance, and the hydrogen diffusion resistance, as was indicated earlier. Similarly, the variation of the intrinsic resistance with hydrogen content can also be obtained during the GIT measurements. The intrinsic resistance of hydride electrode as measured at open circuit using a constant current through the electrode must correspond to the electronic resistance of the MH alloy, the contact resistance be-

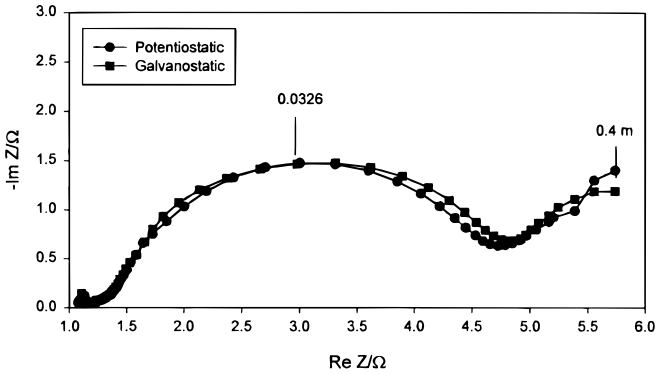

Figure 14. Nyquist plots showing reaction impedance of $LaNi_{4.4}Sn_{0.25}$ electrode using ac with 0.5 mA amplitude or av with 5 mV amplitude.

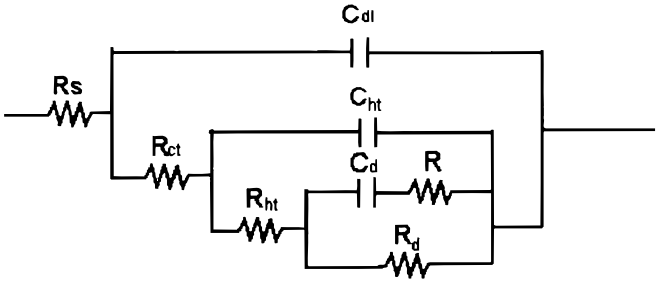

Figure 15. Proposed equivalent circuit of reaction impedance for hydride electrodes.

S0013-4651(99)11-004-8 CCC: $7.00

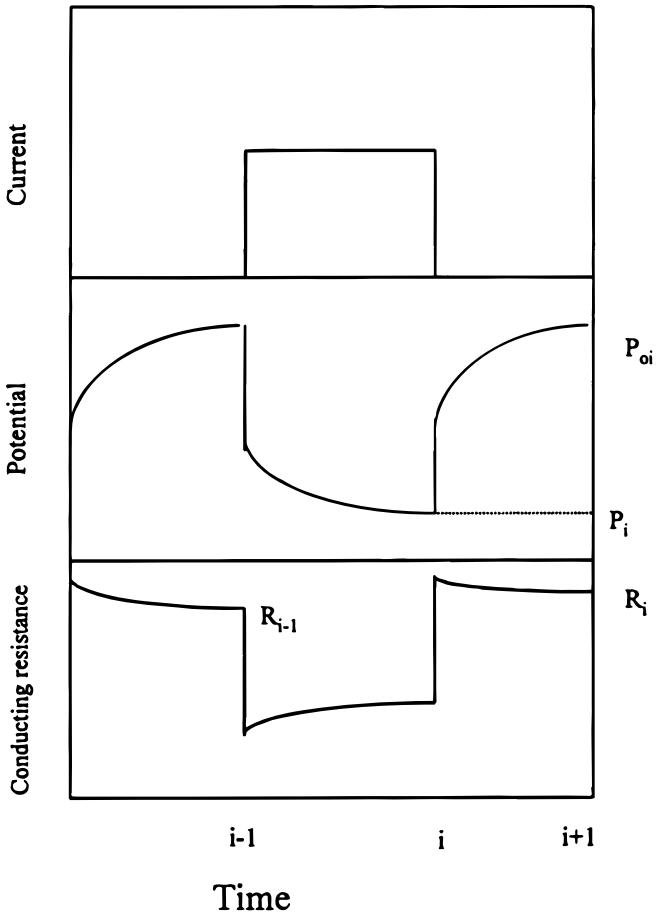

Figure 16. Typical potential and resistance decay curves for a $LaNi_{4.4}Sn_{0.25}$ electrode by microcurrent pulse measurement. Dehydrating reaction resistance at hydrogen content of C_i can be calculated using $R_{ri} = P_i - P_{oi}/I = P_i - P_{oi}/0.00188$.

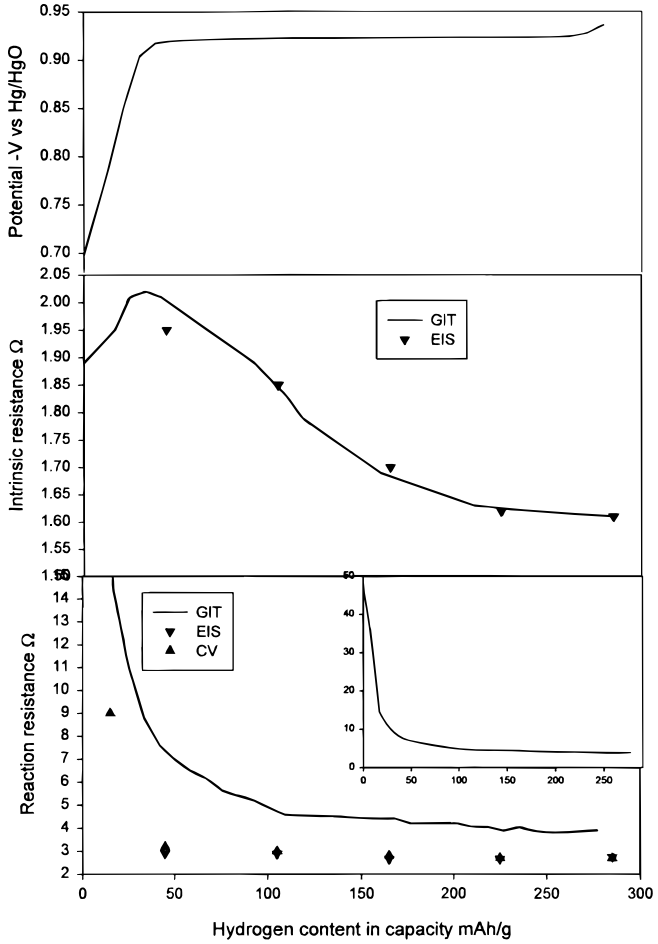

Figure 17. Variation of resistance with hydrogen content for $LaNi_{4.4}Sn_{0.25}$ electrode using microcurrent pulse, EIS, and SACV measurements.

tween the current collector and the local alloy-binder particles, and the particle to particle resistance via the binder.

Figure 17 shows the equilibrium potential, reaction resistance, and intrinsic resistance changes for the discharge of the $LaNi_{4.4}Sn_{0.25}$ electrode before compression. The reaction resistance and intrinsic resistance determined from the EIS data in Fig. 9 and 10 using the equivalent circuit in Fig. 15 and the code Zview (Version 1.4, Scribner Associates, Inc.) are also shown in Fig. 17 for comparison. The reaction resistance increases with decrease in hydrogen content, and its form is almost a mirror image of that of the potential-hydrogen content curve. The rapid increase in reaction resistance at low hydrogen contents results from the high hydrogen diffusion overpotential. However, the intrinsic resistance first increases with decrease in hydrogen content, and then decreases in the low hydrogen content region. This may indicate that the electrical resistance of $LaNi_{4.4}Sn_{0.25}$ alloy is lower than that of $LaNi_{4.4}Sn_{0.25}H_x$. The intrinsic resistances measured during GIT and by EIS are very similar. However, the reaction resistances measured during GIT are higher than those from the EIS because the hydrogen diffusion resistances are not included in the latter. The difference between the two reaction resistances should therefore equal the hydrogen diffusion resistance.

SACV.—SACV was performed under potentiodynamic conditions at a scan rate of 1 mV/s to measure the reaction resistance. Figure 18 shows SACV curves in the fully charged and nominally fully discharged states (*i.e.*, after a 270 mAh/g discharge) of a $LaNi_{4.4}Sn_{0.25}$ electrode before compression. The curves are not strictly linear, and the current hysteresis between anode and cathode scanning increases with increasing SOD. The current hysteresis is caused by the effect of charge and discharge on the three capacitances in the Fig. 15 equivalent circuit. When a voltage scan of k V/s is applied to a resistance in parallel with a capacitance, the current used to charge-discharge the capacitance is $I = \pm (C \times k)$, where $\pm$ indicates charge and discharge. This results in transient processes during voltage scans and capacitance and scan rate dependent current hysteresis equal to 2 Ck. Resistance is therefore best measured from the *V-I* tangent at the end of the charge-discharge transient, as Fig. 18 shows. However, if the capacitive current is a high percentage of the total, (*i.e.*, most of the current is for charging), the value of the parallel resistance cannot be measured and the charge-discharge transient time may be longer than the scan time in each direction. The reaction resistances measured from SACV are also shown in Fig. 17. This reaction resistance is similar to the total resistance obtained from EIS measurements, but lower than that for microcurrent pulse measurement. Zhang *et al.* also found that the total resistances of $LaNi_{4.25}Al_{0.75}$ electrodes determined from linear polarization curves at a low SOD agree with the total resistances obtained from EIS measurements.[7] The present results show that the hydrogen diffusion resistance cannot be measured from SACV (or linear polarization) techniques. C_{ht}, C_{dl}, and C_d determined using Zview are around 0.4, 1.8, and 200 F, respectively, C_d being fitted from the data obtained using the dc method in Fig. 14. From the expression $I = C \times k = 1 \times C$, the charging-discharging currents I_{ht}, I_{dl}, and I_d associated with the above capacitances are 0.4, 1.8, and 200 mA respectively. The current at 10 mV overpotential in Fig. 18 is higher than 1.8 mA, but much less than 200 mA, which indicates that part of the currents are used to charge/discharge to C_{ht} and C_{dl}, but all are

S0013-4651(99)11-004-8 CCC: $7.00

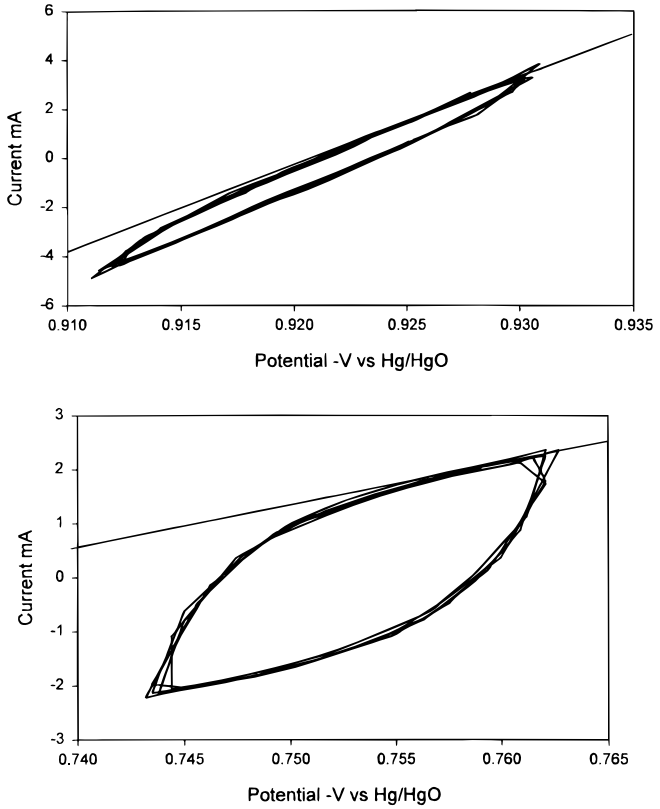

Figure 18. SACV of $LaNi_{4.4}Sn_{0.25}$ electrode at different states of charge at a scan rate of 1 mV/s. (a, top) Fully charged. (b, bottom) With 270 mAh/g discharged.

used to charge-discharge the hydrogen diffusion capacitance C_d. Therefore, cyclic microvotammetry at scan rates under 1 mV/s can only be used to measure the total impedance of the hydrogen transition and charge transfer reactions in this system, and it cannot include the hydrogen diffusion impedance. Reducing the scan rate *k* can decrease the influence of capacitance, which will increase the measured resistance, as Fig. 19 shows. However, very slow potentiodynamic scan rates may change the SOD because of the long measurement time and the flat potential plateau of this alloy electrode. Use of current scanning may solve this problem. Figure 19 also shows the variation of the reaction resistance with current scan rate, which is less than that for voltage scans.

Conclusions

In situ resistance measurements and microperturbation techniques (microcurrent pulse, small amplitude cyclic voltammetry, and electrochemical impedance spectroscopy) have applied to investigate time-dependent charge-discharge behavior and kinetics of the $LaNi_{4.4}Sn_{0.25}$ hydride electrode. Rapid pulverization during the initial electrochemical activation process increased its discharge capacity, although it also increased the contact resistance of the electrode. The decline in capacity resulted from a reduction in hydrogen absorption capability.

Nyquist plots for $LaNi_{4.4}Sn_{0.25}$ electrodes consisted of two semicircles and a slope related to the hydrogen diffusion impedance. The semicircle in the middle frequency region was attributed to charge transfer. In contrast to generally accepted views, the semicircle in the high frequency region seems to relate to the hydrogen transition between absorbed and adsorbed states, and has no relationship with the contact resistance between the current collector and the alloy powder pellet, which certainly exists in hydride electrodes. The

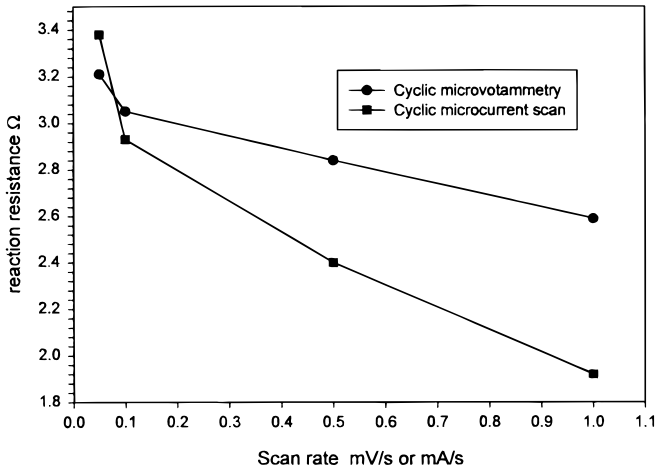

Figure 19. Dependence of reaction resistance for $LaNi_{4.4}Sn_{0.25}$ electrode on scan rate. Reaction resistances measured by av and ac.

semicircle due to infinite hydrogen diffusion in hydride particles can be obtained in a much lower frequency range by using alternating current (ac) instead of av signals for EIS measurement.

For MH electrodes with a flat potential plateau, the total dehydriding reaction resistance, including the resistance of the electrolyte, hydrogen transition from the absorbed to the adsorbed state and the charge transfer reaction and hydrogen diffusion resistances, can be obtained by microcurrent pulse measurements. It is difficult to obtain the hydrogen diffusion resistance from av impedance and cyclic microvoltammetry measurement at overpotentials less than 10 mV and scan rates of 1 mV/s.

Acknowledgments

The authors thank one reviewer for his constructive comments and the suggestion that testing for the stability of the hydride electrode may be performed by reverse frequency sweep and testing for linearity by using different values of the excitation voltage.

Texas A&M University assisted in meeting the publication costs of this article.

References

1. (a) J. J. G. Willems, *Philips J. Res.*, **39,** 1 (1984); (b) J. J. G. Willems and K. H. J. Buschow, *J. Less-Common Met.*, **129,** 13 (1987).
2. Q. M. Yang, M. Ciureanu, D. H. Ryan, and J. O. Strom-Olsen, *J. Electrochem. Soc.*, **141,** 2108 (1994).
3. P. H. L. Notten and P. Hokkeling, *J. Electrochem. Soc.*, **138,** 1877 (1991).
4. B. V. Ratnakumar, C. Witham, R. C. Bowman, Jr., A. Hightower, and B. Fultz, *J. Electrochem. Soc.*, **143,** 2578 (1996).
5. G. Zheng, B. N. Popov, and R. E. White, *J. Electrochem. Soc.*, **143,** 435 (1996).
6. M. Geng, J. Han, F. Fenf, and D. O. Northwood, *J. Electrochem. Soc.*, **146,** 2371 (1999).
7. G. Zheng, B. N. Popov, and R. E. White, *J. Appl. Electrochem.*, **28,** 381 (1998).
8. W. Zhang, M. P. S. Kumar, and S. Srinivasan, *J. Electrochem. Soc.*, **142,** 2935 (1995).
9. C. S. Wang, M. P. Soriaga, and S. Srinivasan, *J. Power Sources*, **85**, 212 (2000).
10. C. S. Wang, *J. Electrochem. Soc.*, **145,** 1801 (1998).
11. A. Lundqvist and G. Lindbergh, *Electrochim. Acta*, **44,** 2523 (1999).
12. N. Kuriyama, T. Sakai, H. Miyamura, I. Uehara, and H. Ishikawa, *J. Alloys Compd.* **202,** 183 (1993).
13. N. Kuriyama, T. Sakai, H. Miyamura, I. Uehara, H. Ishikawa, and T. Iwasaki, *J. Electrochem. Soc.*, **139,** L72 (1992).
14. D. D. Macdonald, *J. Electrochem. Soc.*, **125,** 1977 (1998).
15. C. Jordy, A. Percheron-Guegan, J. Bouet, P. Sanchez, C. Chanson, and J. Leonardi, *J. Less-Common Met.*, **172-174,** 1236 (1991).
16. T. Sakai, H. Miyamura, N. Kuriyama, A. Kato, K. Oguro, and H. Ishikawa, *J. Electrochem. Soc.*, **137,** 795 (1990).
17. C. Iwakura, T. Asaoka, H. Yoneyama, T. Sakai, K. Oguro, and H. Ishikawa, *Nippon Kagaku Kaishi*, 1482 (1988).
18. A. J. Bard and L. R. Faulkner, *Electrochemical Methods, Fundamentals and Applications*, Wiley & Sons, New York (1980).
19. W. L. Zhang, A. Visintin, S. Srinivasan, A. J. Appleby, and H. S. Lim, *J. Power Sources*, **75,** 84 (1998).